(Received 20 May 2024, Accepted 12 August 2024, Scheduled 22 August 2024)

Dual Higher-Order Orbital Angular Momentum Antenna Based on Rectangular Waveguide

Na Li[1,*], Lingling Jiao[2], Guirong Feng[3], Ping Li[4], and Xiaowei Shi[4]

[1]*Shool of Electronic Engineering, Xidian University, Xi'an 710071, China*
[2]*Academy of Advanced Interdisciplinary Research, Xidian University, Xi'an 710061, China*
[3]*Shool of Electronic Engineering, Xi'an University of Posts and Telecommunications, Xi'an 710071, China*
[4]*National Key Laboratory of Antennas and Microwave Technology, Xidian University, Xi'an 710071, China*

ABSTRACT: This paper proposes an antenna based on a rectangular waveguide to generate dual higher-order orbital angular momentum (OAM) beams. The OAM beams with modes $l = -6$ and $l = -7$ are produced by radiating the higher order TE_{mn} transmitted in the rectangular waveguide through a slot. The measurement results indicate that the impedance bandwidth of less than -10 dB is approximately 37.8% in the range of 15–22 GHz, and the mode purity of the antenna is above 55%. The proposed antenna feed structure is simple and does not require a complex phase-shifting network to generate multi-mode and higher-order OAM beams. Such an OAM-based antenna with dual higher-order OAM beams can be utilized in MIMO-OAM communication systems, radar imaging systems, and rotational speed measurement systems.

1. INTRODUCTION

Orbital angular momentum (OAM) has garnered significant attention for providing additional degrees of freedom in modulating electromagnetic waves. In 2012, [1] successfully utilized two OAM modes, $l = 0$ and $l = +1$, to conduct OAM multiplexing communication experiments with a transmission distance of 442 m, marking the inception of radio frequency (RF) OAM communication systems. Building on this progress, in 2021, [2] developed a complex communication technology that integrated OAM-multiple-input multiple-output (MIMO)-polarization. By combining OAM and polarization orthogonality, the device achieved wireless transmission speeds of 117 Gb/s at 40 GHz over a distance of 200 meters. The multiplexing capability of OAM beams has partially alleviated the issue of limited spectrum resources in wireless communication. Moreover, the wave vector characteristics of OAM beams in azimuth induce a rotating doppler effect on reflections from rotating objects. This phenomenon can be harnessed to measure the rotational speed of objects [3, 4]. Importantly, the precision of this measurement is solely dependent on the rotational speed and the order of the OAM beam; it remains unaffected by operational frequency. Multi-mode and high-order OAM beam generation is a prerequisite for these applications.

In order to take advantage of the orthogonality of OAM modes, antenna designs tend to produce OAM beams with multiple modes. Because electromagnetic theory and a generation model for OAM beam-producing antennas are insufficient, generating multi-mode [5] or higher-order modes [6] is challenging, let alone simultaneous. A few antennas have been proposed thus far to generate multi-mode OAM waves, such as uniform concentric circular array (UCCA) [7], metasurface [8, 9], metallic traveling-wave ring-slot antenna [10], solid cylinder dielectric resonator antenna [11], tri-mode concentric circularly polarized patch antenna [12], time-switched array antenna [13], and SPPs [14]. However, the antennas mentioned above have a maximum mode of $+4$, and all have narrow bandwidths.

This paper demonstrates a circularly bent rectangular waveguide loaded with a horn-shaped slot to produce OAM beams with modes $l = -6$ and $l = -7$. The proposed antenna is theoretically designed, fabricated, and measured. The mode purity is above 55%, and the impedance bandwidth of less than -10 dB is approximately 37.8% in the range of 15–22 GHz. The wide impedance bandwidth and simple feed structure of a single port feed make it attractive in practical applications.

2. ANTENNA CONFIGURATION

The construction of the antenna is illustrated in Figure 1. The rectangular waveguide, with a wide side of 18 mm and a narrow side of 8 mm, is bent and joined end to end to form a ring waveguide. According to the theory of rectangular waveguides, TE_{mn} waves in the waveguide are distributed throughout the ring. When an annular current with a phase change of $2\pi l$ is emitted by the slot on the wide side of the waveguide, an OAM beam with mode l is formed. The coaxial probe is used for feeding, saving the waveguide component for coupling, and impedance matching is achieved by adjusting the length of the probe. Additionally, a metal wall is inserted between the two feed ports to ensure that electromagnetic waves travel in the intended direction from port 1 to port 2 along the ring.

The width of the slot increases steadily with transmission distance, starting narrow and becoming wider towards the end to

* Corresponding author: Na Li (lina_xidian@stu.xidian.edu.cn).

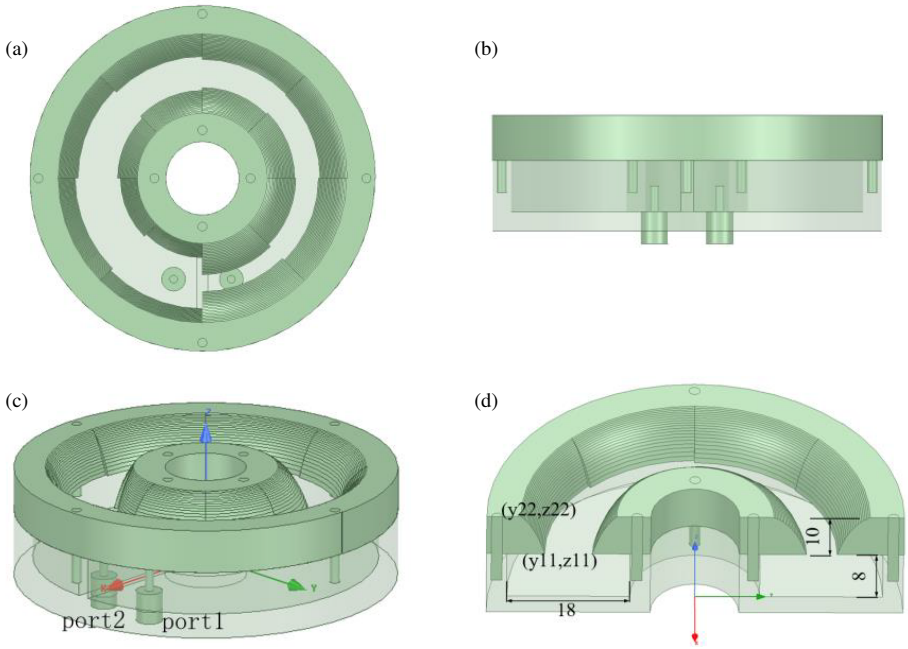

FIGURE 1. Antenna configuration. (a) The top view; (b) the side view; (c) oblique view; and (d) sectional view.

ensure a constant amplitude of the transmitted electromagnetic field. The shape of the slot is determined by parametric Equation (1). $W_{\min}$ represents the minimum width of the slot at the beginning, while $W_{\max}$ represents the maximum width at the end. Specifically, $W_{\min}$ is 3 mm, and $W_{\max}$ is 9 mm. R denotes the distance between the center of the slot and the center of the circular waveguide circle.

$$\begin{cases} x(t) = ((R_1 + (W_{\min}/2)) \cdot \exp((t/2\pi) \\ \qquad \cdot \ln(W_{\max}/W_{\min}))) \cdot \cos t \\ y(t) = ((R_1 + (W_{\min}/2)) \cdot \exp((t/2\pi) \\ \qquad \cdot \ln(W_{\max}/W_{\min}))) \cdot \sin t \end{cases} \tag{1}$$

The slot structure that radiates electromagnetic waves exhibits a significantly narrow impedance bandwidth due to its resonant state. In order to increase the impedance bandwidth, the gap is gradually widened along the z-axis, resulting in the formation of a horn structure with a gradual exponential line shape. The shape of the exponential line is determined by Equations (2)–(4), as shown in Figure 1(d) which depicts the profile of the slot. For ease of manufacturing, the annular slot structure is divided into 8 segments in the φ direction, with both the beginning and end parts having identical widths.

$$Z(x) = C1 \cdot \exp(a \cdot y) + C2 \tag{2}$$

The curve's starting point $(y11, z11)$ and end point $(y22, z22)$ are put into Eq. (2), resulting in $C1$ and $C2$.

$$C1 = \frac{z22 - z11}{\exp(q \cdot y22) - \exp(q \cdot y11))} \tag{3}$$

$$C2 = \frac{z22 \cdot \exp(q \cdot y11) - z11 \cdot \exp(q \cdot y22)}{\exp(q \cdot y11) - \exp(q \cdot y22)} \tag{4}$$

where $(x11, z11)$ and $(x22, z22)$ represent the starting point and end point of the curve, respectively.

The fundamental mode of the rectangular waveguide is TE_{10}, where the electric field component E_z is zero, and the electric field E_x can be represented as

$$E_x = \frac{-jw\mu a}{\pi} A_{10} \sin\left(\frac{\pi x}{a}\right) e^{-j\beta z} \tag{5}$$

That is, E_x has a sinusoidal distribution in the radial direction of the circular waveguide, and E_x propagates in the azimuthal direction of the circular waveguide. The annular waveguide has an inner diameter of 6.5 mm. The rectangular waveguide has a wide side of 18 mm and a narrow side of 8 mm, with a cutoff frequency of $f_{c10} = \frac{c}{2a} = 8.33$ GHz. The cutoff frequencies for the two higher order modes are as follows: TE_{20} is 16.67 GHz, and TE_{11} is 20.51 GHz.

The direction of current on the continuous gap of the waveguide is seen in Figure 2. This current is known as traveling wave

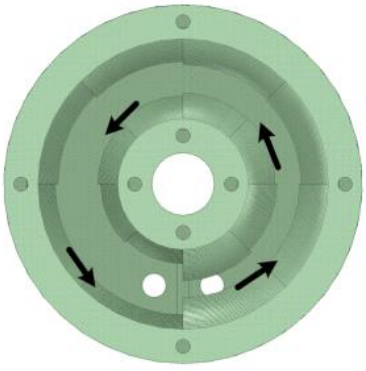

FIGURE 2. The current direction on the continuous slot.

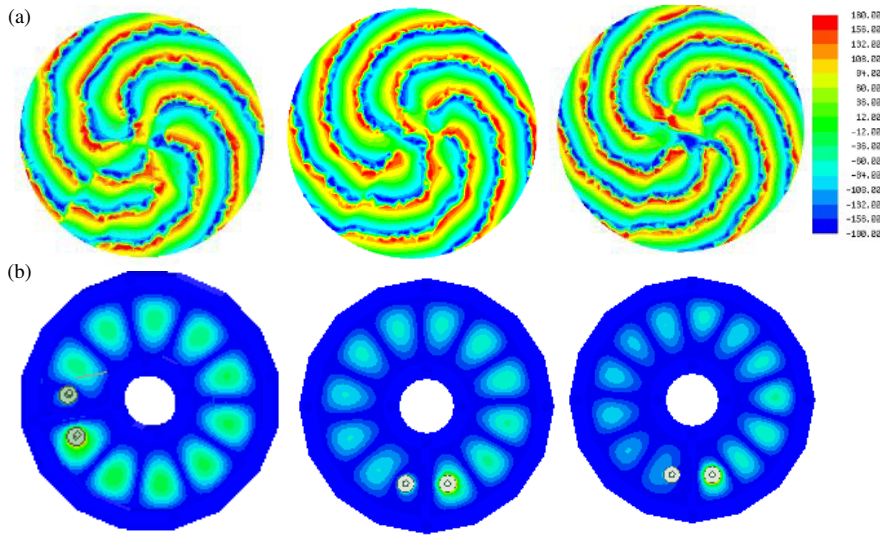

FIGURE 3. (a) Simulated phase distribution and (b) the electric field intensity distribution from left to right are 17.2 GHz, 18.3 GHz, and 20 GHz.

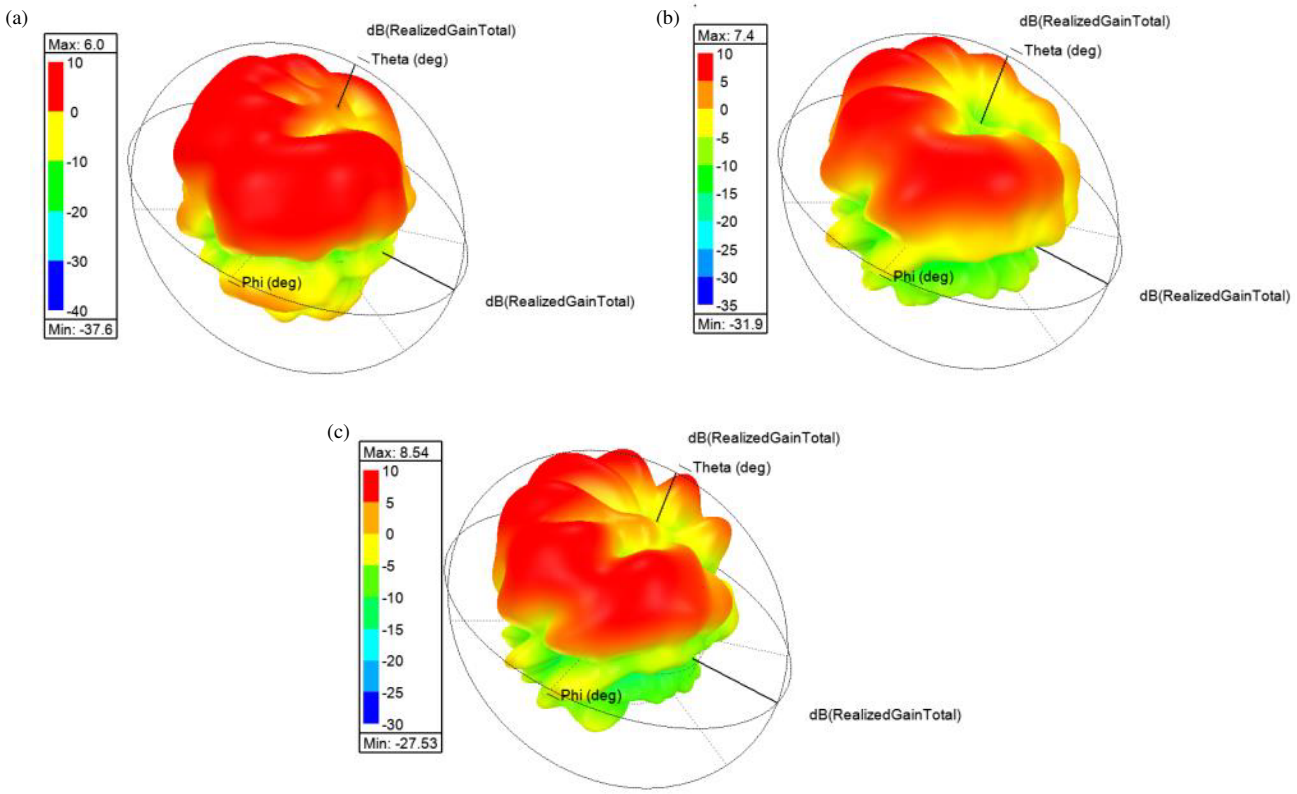

FIGURE 4. Simulated far-field radiation pattern. (a) 17.2 GHz, (b) 18.3 GHz, (c) 20 GHz.

current, and it can be used to create an OAM beam [15]. To compensate for the phenomenon of uneven radiation, the slot structure employs two spiral curves that change in the opposite direction, causing the electromagnetic wave transmitted along the propagation path to increase slowly. In the case of the slot, the current direction is tangential. The waveguide has an average inner and outer diameter of 15.5 mm and a circumference of approximately 97.34 mm, which corresponds to 5.6 wavelengths for 17.2 GHz electromagnetic waves, 5.9 wavelengths for 18.3 GHz electromagnetic waves, and 6.5 wavelengths for 20 GHz electromagnetic waves. Figure 3 provides verification of this. Thus, an OAM beam of mode 6 is formed at 17.2 GHz and 18.3 GHz, whereas an OAM beam of mode 7 is generated at 20 GHz.

3. RESULTS

Figure 3 illustrates the phase distribution of the rectangular waveguide's higher order mode on the observation plane and the simulated electric field intensity distribution within the

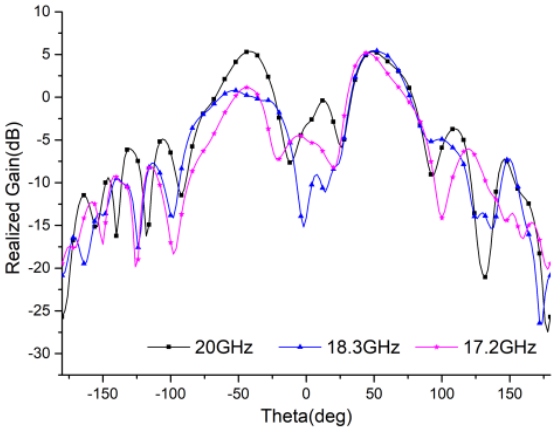

FIGURE 5. Simulated far-field radiation pattern.

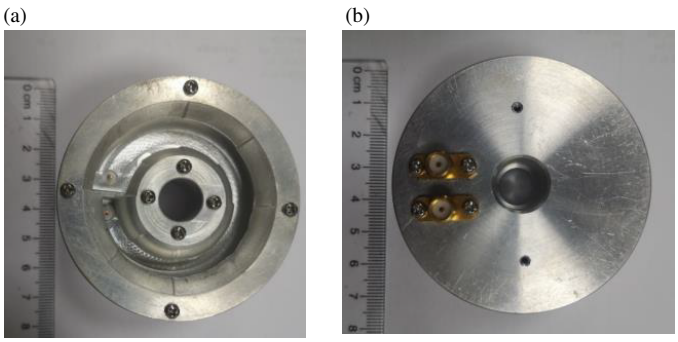

FIGURE 6. The photos of the manufactured antenna. (a) The top view. (b) The bottom view.

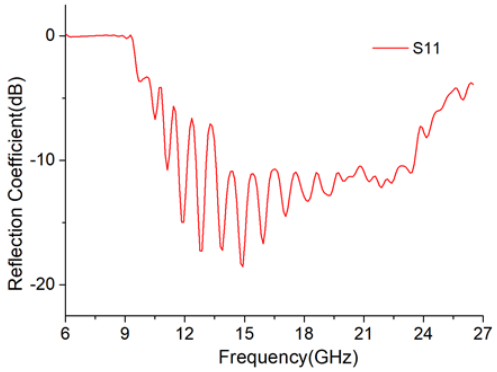

FIGURE 7. The reflection coefficient of the input port.

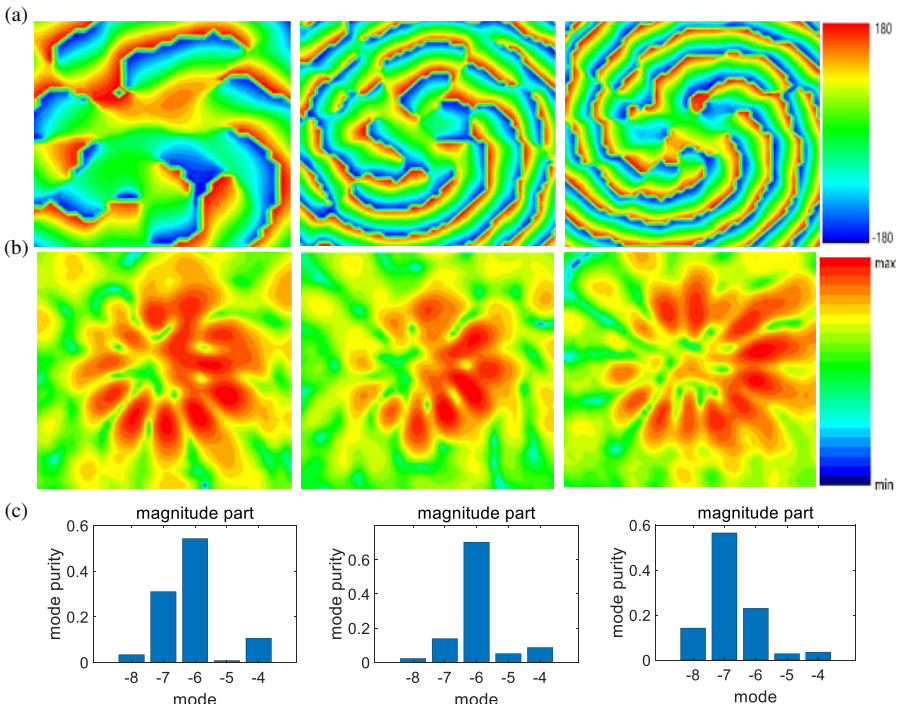

FIGURE 8. (a) Measured the phase distribution, (b) measured the electric field intensity distribution, and (c) the mode purity from left to right are 17.2 GHz, 18.3 GHz, and 20 GHz.

waveguide. The observation surface is a 60 mm radius circle located 30 mm from the antenna surface. It can be observed in Figure 3 that OAM modes -6 and -7 can be generated within the impedance bandwidth. The electric field strength indicates that the higher order mode transmits $l\lambda$ times in the waveguide at the relevant frequency, resulting in the generation of an OAM beam with mode l at various frequencies.

The simulated 3D far-field radiation patterns of the suggested antenna are displayed in Figure 4. The 2D radiation patterns on the antenna's xz plane are concurrently displayed in Figure 5 to provide a deeper understanding of the antenna radiation fields. The results show that the maximum radiation occurs in the direction of $\theta = 50°$ and that there is a clearly deep null at the z axis, indicating that the power density is zero along the propagation axis. Because of its inconsistent amplitude along the ring, the pattern beam produces an asymmetric radiation pattern, making it less than optimal.

Figure 6 depicts photos of the manufactured antenna. The signal is transmitted through the input port, while the terminal port is utilized to match the load during measurement. In Figure 7, the reflection coefficient of the antenna is displayed, indicating an impedance bandwidth of up to 37.8% for $S_{11} < -10$ dB, spanning from 15 GHz to 22 GHz. Figure 8 presents the measured phase distribution of the antenna on a rectangular observation surface measuring $70 * 70$ mm and situated 30 mm away from the antenna surface. Additionally, it displays both mode purity and electric field intensity distribution on this viewing surface. The analysis in Figure 8 reveals that the antenna has capabilities to generate OAM beams at frequencies of 17.2 GHz, 18.3 GHz, and 20 GHz with corresponding modes of -6, -6, and -7, respectively. However, it is noted that mode purity is low due to the inconsistency of the electric field intensity on the ring. To address this issue, adjustments can be made by optimizing slot position and slot equation curve in order to enhance mode purity.

4. CONCLUSION

In conclusion, we have demonstrated the feasibility of an OAM antenna based on a waveguide slot structure for multi-mode and high-mode OAM beams. The antenna impedance band is wide, and the feed network can be easily constructed with coaxial connectors, making it easy to integrate into millimeter wave communication systems. Furthermore, we have developed a prototype and conducted measurements on the OAM modes $l = -6$ and $l = -7$. This antenna shows great potential for applications in target detection and millimeter wave wireless communication systems.

REFERENCES

[1] Tamburini, F., E. Mari, A. Sponselli, B. Thidé, A. Bianchini, and F. Romanato, "Encoding many channels on the same frequency through radio vorticity: First experimental test," *New Journal of Physics*, Vol. 14, No. 3, 033001, 2012.

[2] Yagi, Y., H. Sasaki, T. Semoto, T. Kageyama, T. Yamada, J. Mashino, and D. Lee, "Field experiment of 117 Gbit/s wireless transmission using OAM multiplexing at a distance of 200 m on 40 GHz band," in *2021 IEEE International Conference on Communications Workshops (ICC Workshops)*, 1–5, Montreal, QC, Canada, 2021.

[3] Yang, T. and G. Wang, "Rotational Doppler shift for electromagnetic waves carrying orbital angular momentum based on spectrum analysis," *AIP Conference Proceedings*, Vol. 1820, No. 1, 090024, 2017.

[4] Zheng, J., S. Zheng, Z. Shao, and X. Zhang, "Analysis of rotational Doppler effect based on radio waves carrying orbital angular momentum," *Journal of Applied Physics*, Vol. 124, No. 16, 164907, 2018.

[5] Zhang, Y.-M. and J.-L. Li, "Analyses and full-duplex applications of circularly polarized OAM arrays using sequentially rotated configuration," *IEEE Transactions on Antennas and Propagation*, Vol. 66, No. 12, 7010–7020, Dec. 2018.

[6] Thidé, B., H. Then, J. Sjöholm, K. Palmer, J. Bergman, T. D. Carozzi, Y. N. Istomin, N. H. Ibragimov, and R. Khamitova, "Utilization of photon orbital angular momentum in the low-frequency radio domain," *Physical Review Letters*, Vol. 99, No. 8, 087701, Aug. 2007.

[7] Lee, D., H. Sasaki, H. Fukumoto, Y. Yagi, T. Kaho, H. Shiba, and T. Shimizu, "An experimental demonstration of 28 GHz band wireless OAM-MIMO (orbital angular momentum multi-input and multi-output) multiplexing," in *2018 IEEE 87th Vehicular Technology Conference (VTC Spring)*, 1–5, Porto, Portugal, Jun. 2018.

[8] Meng, X., J. Wu, Z. Wu, L. Yang, L. Huang, X. Li, T. Qu, and Z. Wu, "Generation of multiple beams carrying different orbital angular momentum modes based on anisotropic holographic metasurfaces in the radio-frequency domain," *Applied Physics Letters*, Vol. 114, No. 9, Mar. 2019.

[9] Shen, Y., J. Yang, H. Meng, W. Dou, and S. Hu, "Generating millimeter-wave bessel beam with orbital angular momentum using reflective-type metasurface inherently integrated with source," *Applied Physics Letters*, Vol. 112, No. 14, 141901, Apr. 2018.

[10] Zhang, W., S. Zheng, X. Hui, Y. Chen, X. Jin, H. Chi, and X. Zhang, "Four-OAM-mode antenna with traveling-wave ring-slot structure," *IEEE Antennas and Wireless Propagation Letters*, Vol. 16, 194–197, 2016.

[11] Liang, J. and S. Zhang, "Orbital angular momentum (OAM) generation by cylinder dielectric resonator antenna for future wireless communications," *IEEE Access*, Vol. 4, 9570–9574, 2016.

[12] Zhang, Z. and S. Xiao, "Generation of multiple orbital angular momentum (OAM) modes with a circularly polarized multimode patch antenna," in *2016 IEEE MTT-S International Wireless Symposium (IWS)*, 1–4, Shanghai, China, Mar. 2016.

[13] Tennant, A. and B. Allen, "Generation of radio frequency OAM radiation modes using circular time-switched and phased array antennas," in *2012 Loughborough Antennas & Propagation Conference (LAPC)*, 1–4, Loughborough, Leicestershire, United Kingdom, Nov. 2012.

[14] Yan, Y., G. Xie, M. P. J. Lavery, H. Huang, N. Ahmed, C. Bao, Y. Ren, Y. Cao, L. Li, Z. Zhao, A. F. Molisch, M. Tur, M. J. Padgett, and A. E. Willner, "High-capacity millimetre-wave communications with orbital angular momentum multiplexing," *Nature Communications*, Vol. 5, No. 1, 4876, Dec. 2014.

[15] Zhang, Z., S. Zheng, X. Jin, H. Chi, and X. Zhang, "Generation of plane spiral OAM waves using traveling-wave circular slot antenna," *IEEE Antennas and Wireless Propagation Letters*, Vol. 16, 8–11, 2017.